

Pre-strain Effect on Frequency-Based Impact Energy Dissipation through a Silicone Foam Pad for Shock Mitigation

Brett Sanborn¹ · Bo Song¹ · Scott Smith²

Received: 29 October 2015 / Accepted: 16 December 2015 / Published online: 29 December 2015
© The authors 2015

Abstract Silicone foams have been used in a variety of applications from gaskets to cushioning pads over a wide range of environments. Particularly, silicone foams are used as a shock mitigation material for shock and vibration applications. Understanding the shock mitigation response, particularly in the frequency domain, is critical for optimal designs to protect internal devices and components more effectively and efficiently. The silicone foams may be subjected to pre-strains during the assembly process which may consequently influence the frequency response with respect to shock mitigation performance. A Kolsky compression bar was modified with pre-compression capabilities to characterize the shock mitigation response of silicone foam in the frequency domain to determine the effect of pre-strain. A silicone sample was also intentionally subjected to repeated pre-strain and dynamic loadings to explore the effect of repeated loading on the frequency response of shock mitigation.

Keywords Kolsky bar · Frequency response · Silicone foam · Energy dissipation · Shock mitigation

Introduction

Silicone foams, also known as silicone rubber foams, have been utilized in many applications such as thermal insulation, vibration reduction, and shock mitigation materials [1–3]. For example, silicone foams have been chosen as a

covering material for sandwich structures subjected to underwater explosion due to their superior shock resistant performance [1]. As a hyperelastic polymer with a cellular structure, polymeric foam exhibits significant effects from temperature, strain rate, and stress state on the mechanical stress–strain responses [4, 5]. The changes in the stress–strain response further result in different (better or worse) shock mitigation performance against external impacts, shocks, or explosions. For instance, the shock mitigation performance of silicone foams may depend on environmental and loading conditions as well as stress states. In addition, silicone foams are inevitably subjected to preload during assembly processes, which may also result in a change of their shock mitigation performance to the assembled components.

A general principle for better shock mitigation of a foam material is to maximize the total amount of shock energy absorption but with minimized transmitted force and acceleration. The total amount of energy that can be absorbed through a foam material has been calculated with the area in the stress–strain curve prior to densification of the foam material [4]. This energy calculation only represents the energy absorption capacity of the specific foam material without providing any information with respect to frequency response. The frequency response of shock mitigation materials has been less investigated, due to both experimental and analytical difficulties, but is critical to predict the survivability and functionality of the protected components. Recently, Song and Nelson [6] employed Kolsky compression bar (also called split Hopkinson pressure bar, SHPB) techniques and developed frequency-based analyses to investigate the frequency response of impact energy absorption of a polymethylene diisocyanate (PMDI) based rigid polyurethane foam. Their results showed that nearly all impact energy above the

✉ Brett Sanborn
bsanbor@sandia.gov

¹ Sandia National Laboratories, Albuquerque, NM 87185, USA

² The University of Georgia, Athens, GA 30602, USA

characteristic frequency (1.5 kHz) was absorbed by the PMDI foam under nearly uniaxial compression load and without any preload, even though the characteristic frequency might depend on the stress state and preload conditions [6].

As a soft hyperelastic material, silicone foams can be easily deformed even under a small amount of force, during assembly processes of shock mitigation systems [7], which may cause the pre-strained silicone foam to behave differently in shock mitigation applications. However, no experiment has been executed to investigate the pre-strain effect on the shock mitigation response, particularly in the frequency domain, of silicone foams. Proper modification to current experimental techniques is thus required to generate pre-loads to the specimen before dynamic loading, though the Kolsky compression bar has been demonstrated to characterize shock response of foam materials [6]. In fact, the preload capability has been implemented to Kolsky tension bars [8, 9]; however, the same preload capability is not applicable to Kolsky compression bars. A new design of preload capability for Kolsky compression bars is thus required.

When used as a shock mitigation pad in components, the silicone foam is usually laterally confined and subjected to a triaxial stress state. This may also result in a different frequency response of shock mitigation. Therefore, in order to appropriately understand the frequency response in shock mitigation applications, dynamic experiments are recommended for pre-strained and confined silicone foams with proper frequency-based analyses.

In this study, a Kolsky compression bar was modified with pre-compression load capability. The silicone foam samples were laterally confined and pre-strained to different levels before dynamic loading. The frequency-based analyses developed by Song and Nelson [6] were applied to characterize the frequency response of shock mitigation of the silicone foams pre-strained to different levels. The effect of pre-strain on the frequency response of shock mitigation through the silicone foam was then determined.

Material and Specimens

The material investigated in this study was open cell silicone foam with a non-compressed density of $608 \pm 21.85 \text{ kg/m}^3$. The silicone foam, which had an average size of $\sim 0.5 \text{ mm}$ (Fig. 1), is a highly flexible and compressible foam material. The silicone foam specimens had an average diameter of $25.37 \pm 0.08 \text{ mm}$ and an average thickness of $5.33 \pm 0.006 \text{ mm}$. Experiments were conducted at pre-strains of 0, 13, 23.3, and 33.5 % engineering strain. Three experiments were conducted at each condition. For the repeated loading experiments, a

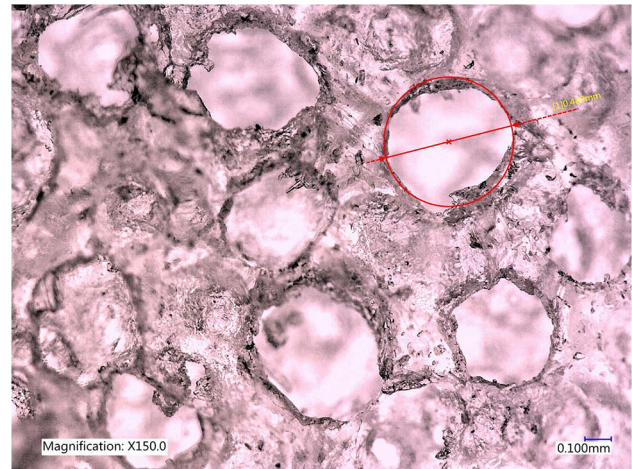


Fig. 1 Optical micrograph of silicone foam

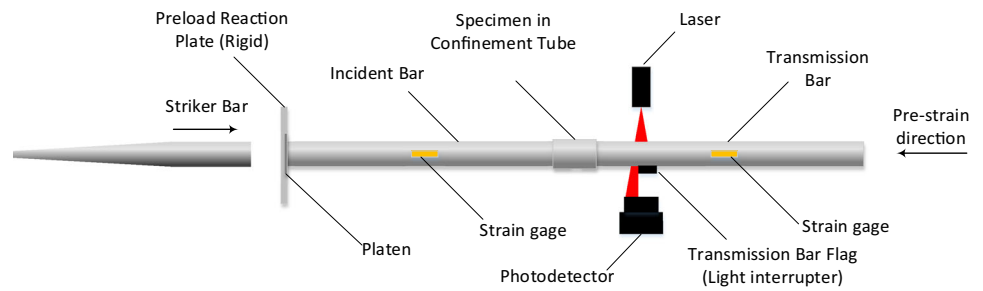
specimen was reloaded five times after an initial loading to determine the effect of repeated loading on the shock mitigation performance.

Kolsky Compression Bar with Pre-load Capability

A standard compression Kolsky bar was modified for the dynamic compression experiments. The standard compression bar system consists of a striker, an incident bar, and a transmission bar as shown in Fig. 2. In this study, the incident and transmission bars were made of C300 maraging steel and had a common diameter of 25.4 mm. Upon impact of the striker on the incident bar, the loading pulse propagates along the incident bar toward the specimen and loads the specimen sandwiched between the incident and transmission bars. In order to generate a high-frequency incident pulse, no pulse shaper was applied to the impact end of the incident bar. In addition, the silicone foam specimens were not lubricated at the bar ends to eliminate the effect of lubricant on the frequency response of the silicone foam material under investigation. The strain gages mounted on the incident and transmission bars were used to record the stress pulse time histories for quantifying the shock mitigation response of the material in the frequency domain through Fourier transformation. Since the silicone foam in this study was such a soft material, the magnitude of the transmitted pulse was two orders of magnitude lower than that of the incident pulse. For this reason, semiconductor strain gages were used on the transmission bar to record the transmitted stress history.

The Kolsky compression bar setup was outfitted with a reaction plate at the impact end of the incident bar as shown in Fig. 2. The reaction plate was machined with a hole and recessed shoulder so that a platen could be loosely

Fig. 2 Schematic of compression bar setup



placed in the reaction plate to prevent the incident bar from moving toward the striker and gun barrel as the specimen was subjected to the pre-strain [10]. Upon impact, the hole and shoulder configuration in the reaction plate allowed the platen to move freely in the same direction (the loading direction) as the striker without impeding the incident pulse from entering the incident bar.

The specimen gage length was measured and a gap of the same size was set between the incident and transmission bars to ensure the specimen in contact with the bar ends but without any pre-strain. The specimen was inserted into the gap and the confinement sleeve was slid over the specimen. The confining sleeve was made of 4340 steel and had an outer diameter of 31.8 mm and an inner diameter of 25.5 mm. A schematic of the specimen contained in the confinement tube is shown in Fig. 3.

A laser extensometer system was used on the transmission bar to accurately determine the amount of pre-strain applied to the specimen prior to dynamic loading [11]. The laser system consisted of a uniform line laser as a light source and a highly sensitive photodetector. A flag was attached to the transmission bar to block the light to the photodetector as the transmission bar was advanced during pre-straining (Fig. 2). The amount of engineering strain applied to the specimen was determined using

$$\epsilon_{pre} = \frac{\Delta L}{L} \tag{1}$$

where L is the original length of the specimen.

Unlike using a cylindrical striker in conventional Kolsky bar tests, a tapered striker made from tungsten alloy

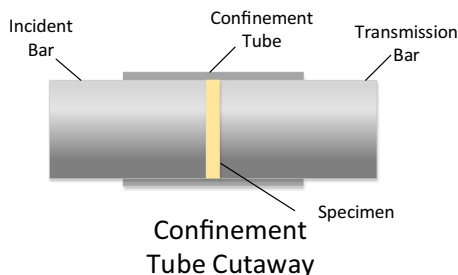


Fig. 3 Specimen in confinement tube to achieve a triaxial stress-state

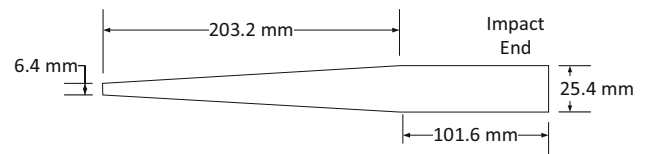


Fig. 4 Tapered striker design

(Figs. 2, 4) was designed and used in this study to generate a pulse with a wide range of frequency content. Tapered strikers have been previously used primarily for pulse shaping purposes [12, 13]. However, the application to this study is to alter the shape of the unloading tail. Upon impact, the striker produces an incident pulse with a fast rise time and long unloading tail. Because the tungsten striker has higher mechanical impedance than the steel incident bar, the incident pulse would normally possess a long step-wise unloading profile [14]. The tapered tail of the tungsten striker created a relatively smooth unloading profile on the incident pulse, as shown in Fig. 5. In Fig. 5, a loading profile using a conventional steel striker is also plotted for comparison. Again, no pulse shaper was used in either case.

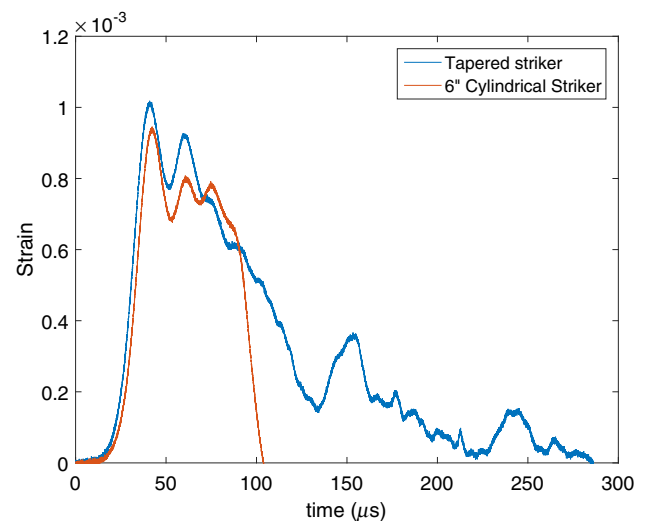


Fig. 5 Pulse generated using the tapered striker compared to a conventional striker

Figure 6 shows comparisons of frequency content in the pulses shown in Fig. 5. The cylindrical steel striker generated a nearly zero magnitude at the frequency of approximately 15 kHz, which made quantitative shock mitigation responses around this frequency unobtainable. However, when using a tapered tungsten striker, this blind frequency is extended to approximately 23 kHz. Therefore, the utilization of the tapered tungsten striker extends the highest frequency that can be probed using the Kolsky bar.

After the time histories for the incident, reflected, and transmitted pulses are recorded, the energies associated with each of the pulses in the frequency domain are calculated to characterize the energy dissipation behavior of the material. Each bar strain signal in the time domain, $\varepsilon(t)$, has the Fourier transform [6]

$$\varepsilon(f) = B(f)e^{-j(2\pi f + \phi)} \tag{2}$$

where $B(f)$, f , and ϕ are the magnitude, frequency, and phase of the Fourier transform. The energy spectrum density in the frequency domain for each of the signals is

$$S_i(f) = A_0 C_0 E_0 |B_i(f)|^2 \tag{3}$$

$$S_r(f) = A_0 C_0 E_0 |B_r(f)|^2 \tag{4}$$

$$S_t(f) = A_0 C_0 E_0 |B_t(f)|^2 \tag{5}$$

where A_0 , C_0 , and E_0 are the bar area, wave speed, and elastic modulus, respectively. $B_i(f)$, $B_r(f)$, $B_t(f)$ are the magnitudes of the Fourier transforms of the incident, reflected, and transmitted pulses, respectively. The corresponding energy dissipation ratio is thus computed as

$$\delta(f) = 1 - \frac{|B_t(f)|^2}{|B_i(f)|^2 - |B_r(f)|^2} \tag{6}$$

Experiments and Results

A typical set of incident and transmission bar signals is shown in Fig. 7, again noting that the transmitted signal was recorded with a pair of semiconductor strain gages; the sensitivity of which is approximately 80 times higher than the resistance strain gages used to record the incident and reflected pulses. As shown in Fig. 7, the transmitted strain signal was approximately 100 times lower than the incident strain signal. However, using the semiconductor strain gages yields a high-resolution measurement of such a weak transmitted strain signal. The total duration of the transmitted signal is much longer than that of the incident pulse. This is because the recovery force of the silicone foam during unloading is too low to accommodate the friction between the pressure bars and bar supports to push them back, showing a “stress relaxation” behavior. Figure 7 shows that that when $t = 1150 \mu s$, the transmitted pulse was overlapped by its reflection at the free end of the transmission bar. In this study, only the loading and stress relaxation behavior before the transmitted signal is reflected back was included in the energy dissipation analysis. The timespan used for the incident and reflected FFT calculations was the same as the overall length of the transmitted pulse.

Similar to conventional Kolsky bar data reduction, the incident, reflected, and transmitted pulses were shifted back to the specimen surfaces, as shown in Fig. 8, for energy dissipation analysis in the frequency domain. Wave

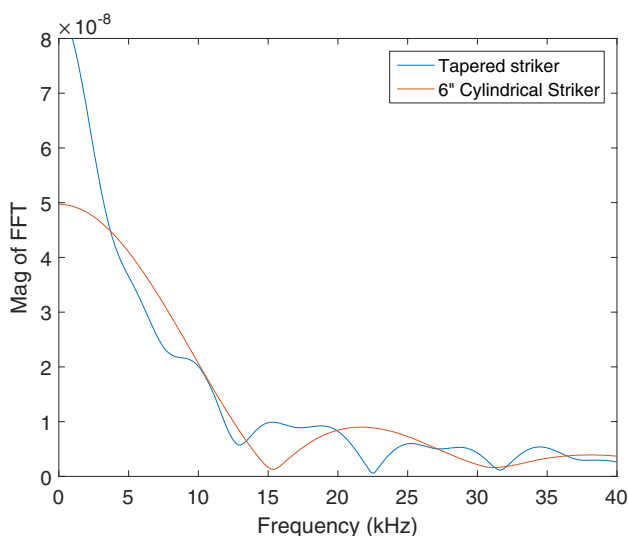


Fig. 6 Comparison of the FFT of the tapered striker to a conventional striker

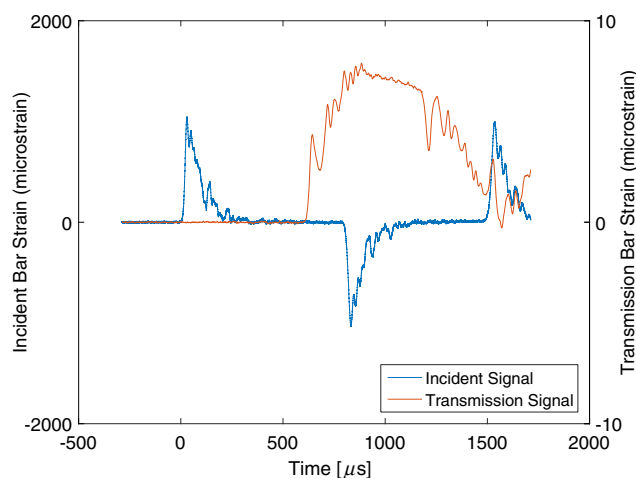


Fig. 7 Oscilloscope records from a Kolsky compression bar experiment on silicone foam subjected to a 33.5 % pre-strain, loaded using a tapered tungsten striker

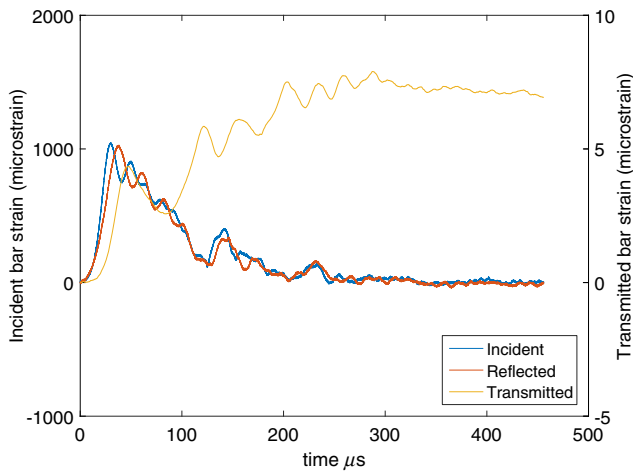


Fig. 8 Isolated incident, reflected, and transmitted pulses

dispersion in experiments is common and needs to be corrected or minimized in conventional Kolsky bar data reduction. However, the wave dispersion is caused by phase changes due to different phase velocities at different frequencies [15], which should not influence frequency analysis. Therefore, the wave dispersion correction is not necessary for frequency analysis in this study.

The energies associated with the incident, reflected, and transmitted signals in Fig. 8 were calculated with Eqs. (3)–(5) and are shown in Fig. 9. As shown in Fig. 9, the energy density of the incident pulse is greater than that of the reflected pulse until a frequency of about 4 kHz where the energy density of the reflected pulse becomes slightly higher. This probably indicates frequency shifts when the stress wave is reflected back. The possible frequency shifts may depend on the mechanical properties of the material under investigation. When the frequency increases to about

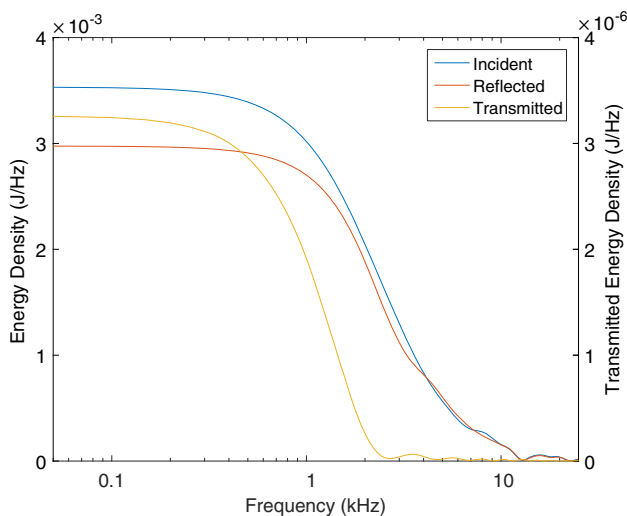


Fig. 9 Energy density of incident, reflected, and transmitted signals

7 kHz, the incident energy density again becomes greater than the reflected energy density. After a frequency of about 10 kHz, the two energy densities are nearly indistinguishable.

Figure 9 also shows that at the frequencies of 4, 7, and 10 kHz, the incident energy density is the same as the reflected energy density, indicating that no energy at these frequencies has been transferred into the silicone foam specimen. This will generate discontinuities of energy dissipation calculated with Eq. (6) at these frequencies, as shown in Fig. 10. Figure 10 shows the frequency spectrum of energy dissipation ratio through the silicone foam pre-strained to 33.5 %. The plot in Fig. 10 shows that the initial energy dissipation ratio is 0.995 until a cutoff frequency of 2.65 kHz is reached, where the dissipation ratio becomes even closer to 1 with a value of 0.9999. These results are likely due to the extreme efficiency of the silicone foam at dissipating applied energy, even at low frequencies. Although the loading and boundary conditions of the specimens were different, earlier work by Song and Nelson [6] on PDMI foam showed less energy dissipation at low frequencies. In that case, the PDMI foam had an initial energy dissipation ratio of 0.87 and reached full dissipation (energy dissipation ratio of 1) at approximately 1.5 kHz. In other words, even though the silicone foam was already pre-strained to 33.5 % in this study, the silicone foam shows much better shock mitigation response across the frequency spectrum.

Following the same procedure, the silicone foams pre-strained to four different levels (0, 13, 23.3, and 33.5 %) were characterized under the same confinement in the time domain and analyzed in terms of shock mitigation in the frequency domain. The loading conditions remained the

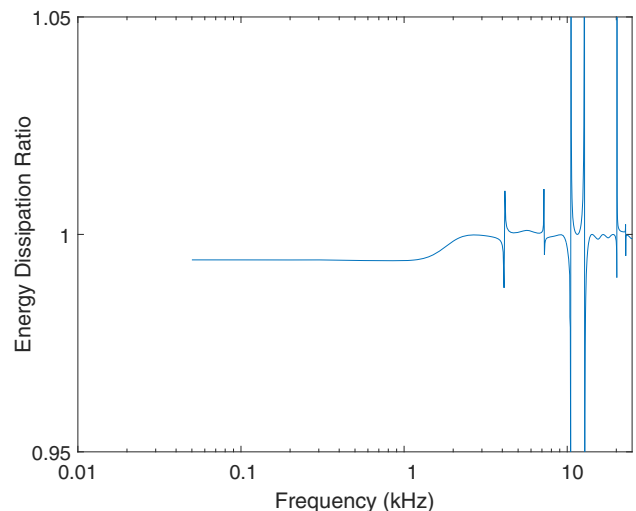


Fig. 10 Energy dissipation ratio of a 33.5 % pre-strained silicone foam sample

same for all mechanical testing. At each condition, three experiments were repeated. Figure 11 shows the transmitted signals for all repeated experiments at each pre-strain condition. The small amount of variation observed at the same condition is due to slight variations in the sample diameter or the amount of applied pre-strain on the sample.

The same frequency-based analyses were then applied and the results are summarized in Fig. 12. In the frequency domain, the energy dissipation behavior was close to 1 for each of the investigated pre-strains, as shown in Fig. 12a. Zooming in further as in Fig. 12b, a trend can be seen where the specimens that were pre-strained to 33.5 % had lower energy dissipation capability compared to the other pre-strains at the frequencies below 2 kHz. Discontinuities in the energy dissipation ratio were observed similar to those discussed in the previous section. In addition, in some cases the energy dissipation ratio was observed to become greater than 1 at the frequencies below 1 kHz (Fig. 12). One possible reason is calculation error. As mentioned earlier, the reflected energy spectral density was first subtracted from the incident energy spectral density to calculate the total input energy density into the specimen. However, due to the nature of very soft silicone foam, the incident and reflected energy spectral densities are very close. This subtraction may generate a significant error, which will be further amplified when it is used to calculate the energy dissipation ratio with Eq. (6). Another reason might be a representation of frequency shift through the soft silicone foam specimen, which is still under investigation. Even though the frequency data in Fig. 12 show scattering and discontinuities at some frequencies, the frequency response of shock mitigation of the silicone foam exhibits dependency on pre-strain. With increasing pre-strain, the energies were dissipated less at low

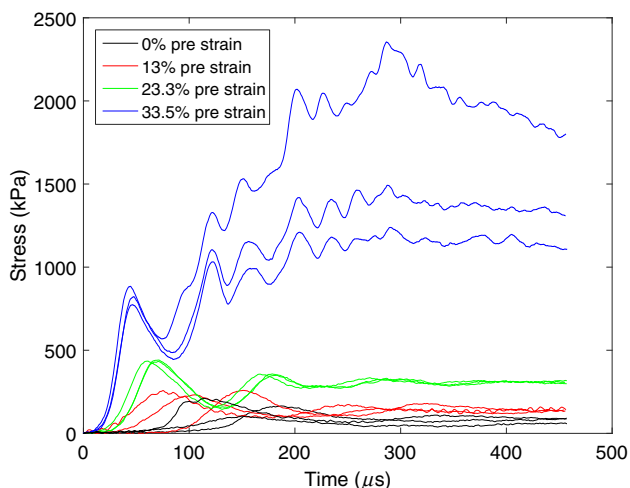


Fig. 11 Stress-time history from silicone foam experiments at different levels of pre-strain

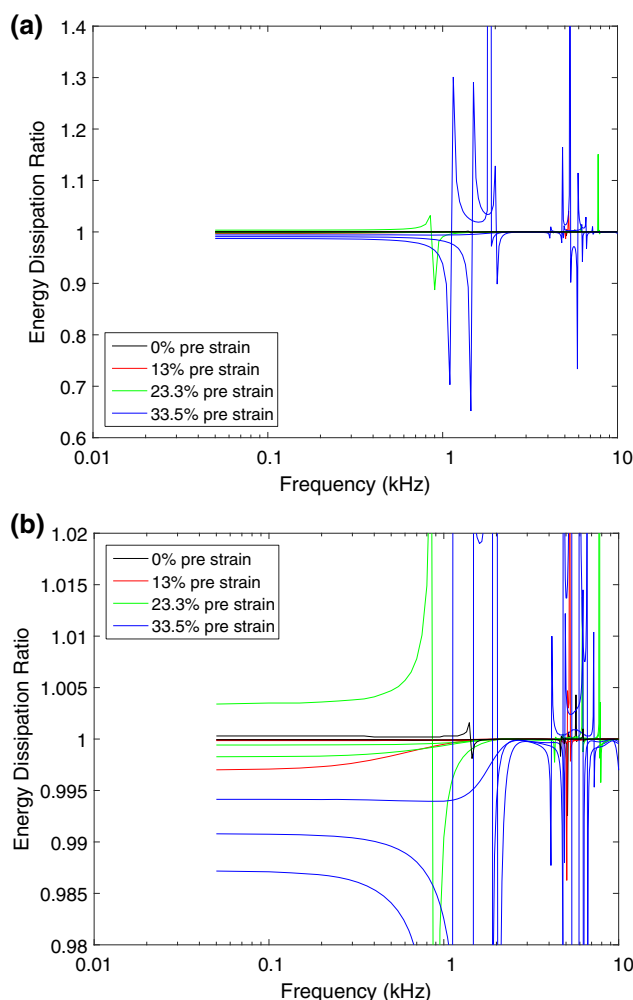


Fig. 12 **a** Energy dissipation behavior of silicone foam at different pre-strains. **b** Zoomed-in plot of the energy dissipation behavior as a function of pre-strain and frequency

frequencies. When the silicone foam was pre-strained to 33.5 %, nearly 99 % of the low-frequency energy was dissipated. However, the total energy dissipation approaches 1 with reduction of pre-strain. Two of the three experiments at 13 % pre-strain were indistinguishable from experiments with no pre-strain. One of the 13 % pre-strain experiments showed slightly lower dissipation at low frequencies (0.997 dissipation) but quickly reached an energy dissipation of 1 at 2 kHz. In addition, the cut-off frequency decreases from 2.65 kHz to below 2 kHz when the pre-strain decreases from 33.5 to 13 %. Nearly all energy at all frequencies was dissipated when the silicone foam was not pre-strained.

To investigate the response of silicone foam to repeated loading in both the time and frequency domains, six repeated loading experiments with the same inputs were conducted on a single silicone foam specimen. In these experiments, the specimen was not subjected to pre-strain.

The stress-time histories from each of these experiments are plotted together in Fig. 13 to show the repeatability of the silicone foam response. The specimen thickness and diameter were also measured following each experiment and were found to vary less than 1 % comparing the initial and final experiments. The recovery time of the silicone foam was not controlled during the experiments. The recovery time varied from minutes to several hours between experiments but the high repeatability observed in Fig. 13 does not indicate that the silicone foam response was sensitive to recovery time.

The energy dissipation response of the silicone foam in the frequency domain was also repeatable, as is shown in Fig. 14, which does not show a significant effect of repeated loading. The silicone foam dissipated nearly all of the loading energy in the frequency domain since the energy dissipation ratio is 1 ± 0.05 %. This is because of the nature of hyperelasticity of this silicone foam.

Conclusions

Modified Kolsky compression bar techniques were used to characterize the shock mitigation response of silicone foam in the frequency domain. A tapered tungsten striker was used to generate an incident pulse with higher frequency components. The silicone foam specimens were laterally confined and subjected to different pre-strains to investigate the effect of pre-strain on the frequency response to mimic possible pre-loads on the shock mitigation material during assembly or manufacturing. Repeated loading experiments were conducted to explore the effect of repeated loading on the frequency response.

The silicone foam investigated in this study was found to be an excellent material for energy dissipation over a

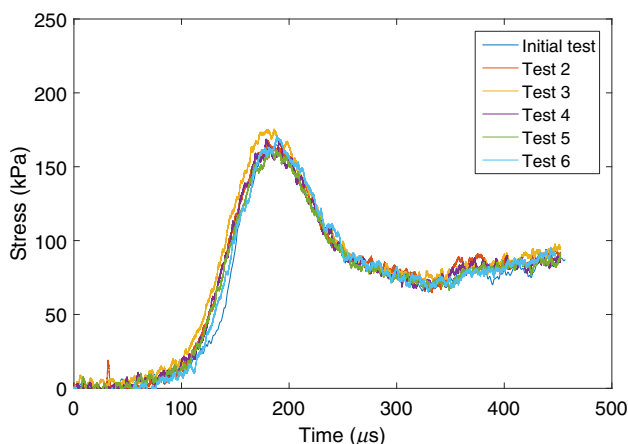


Fig. 13 Stress time history of the repeated loading experiments on silicone foam

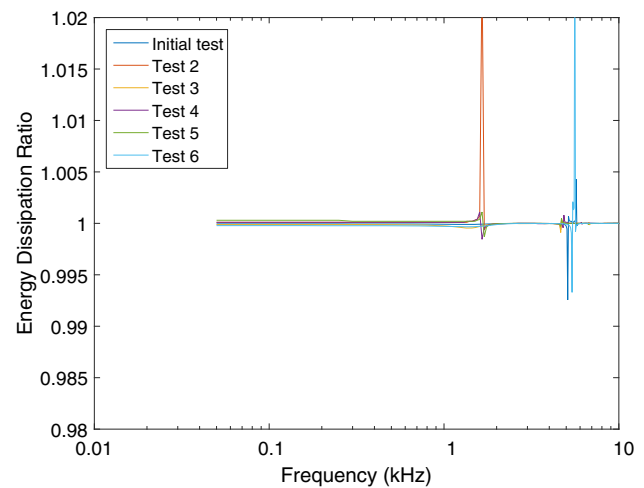


Fig. 14 Energy dissipation of silicone foam samples subjected to repeated loading

wide range of frequencies. Even when pre-strained to 33.5 %, the silicone foam shows better shock mitigation compared to previous work conducted on a PDMI foam. The silicone foam shows increasing energy dissipation with decreasing pre-strain, despite the fact that at 33.5 % pre-strain, 99 % of the energy was dissipated. The cutoff frequency of the silicone foam was observed to decrease from 2.65 kHz to 2 kHz when the pre-strain was decreased from 23.3 to 13 %. Subjected to five repeated loadings, the confined silicone foam dissipated nearly all of the energy over the frequency spectrum under no preload, showing insignificant effect of repeated loading. The results presented here are only valid for the experimental conditions conducted in this study. The silicone foam may dissipate impact energy differently at different loading speeds and higher amounts of pre-strain due to significant nonlinear stress–strain behavior and strain-rate effect.

Acknowledgments Sandia National Laboratories is a multi-program laboratory managed and operated by Sandia Corporation, a wholly owned subsidiary of Lockheed Martin Corporation, for the U.S. Department of Energy’s National Nuclear Security Administration under contract DE-AC04-94AL85000.

References

- Zhang Z, Ming F, Zhang A (2014) Damage characteristics of coated cylindrical shells subjected to underwater contact explosion. *Shock Vib*. doi:[10.1155/2014/763607](https://doi.org/10.1155/2014/763607)
- Rabe JA, Spells S, Rasch DM, Homan GR, Lee CL (1981) Evaluation of silicone foam for flat plate solar collector insulation. *Sol Energy Mater* 4:159–168. doi:[10.1016/0165-1633\(81\)90039-3](https://doi.org/10.1016/0165-1633(81)90039-3)
- Blood RP, Ploger JD, Yost MG, Ching RP, Johnson PW (2010) Whole body vibration exposures in metropolitan bus drivers: a comparison of three seats. *J Sound Vib* 329:109–120. doi:[10.1016/j.jsv.2009.08.030](https://doi.org/10.1016/j.jsv.2009.08.030)

4. Gibson LJ, Ashby MF (1999) Cellular solids, structure, and properties, 2nd edn. Cambridge University Press, Cambridge
5. Song B, Lu WY, Syn CJ, Chen W (2009) The effects of strain rate, density, and temperature on the mechanical properties of polymethylene diisocyanate (PMDI)-based rigid polyurethane foams during compression. *J Mater Sci* 44:351–357. doi:[10.1007/s10853-008-3105-0](https://doi.org/10.1007/s10853-008-3105-0)
6. Song B, Nelson K (2015) Dynamic characterization of frequency response of shock mitigation of a polymethylene diisocyanate (PMDI) based rigid polyurethane foam. *Lat Am J Solids Struct* 12:1790–1806
7. Wang F, Wan F (2013) The dispersion estimation method for assembly stress of silicone rubber foam pad based on extreme value distribution. *Appl Mech Mater* 387:85–89. doi:[10.4028/www.scientific.net/amm.387.85](https://doi.org/10.4028/www.scientific.net/amm.387.85)
8. Song B, Lu WY (2012) Preload high-rate tension techniques In: Proceedings of SEM XII international congress and exposition on experimental and applied mechanics, Costa Mesa, 11–14 June, 2012. doi:[10.1007/978-1-4614-4238-7_24](https://doi.org/10.1007/978-1-4614-4238-7_24)
9. Song B, Nelson K, Lipinski R, Bignell J, Ulrich GB, George EP (2015) Dynamic high-temperature tensile characterization of an iridium alloy with Kolsky tension bar techniques. *J Dyn Behav Mater* 1:290–298. doi:[10.1007/s40870-015-0022-6](https://doi.org/10.1007/s40870-015-0022-6)
10. Chen W, Song B (2011) Split Hopkinson (Kolsky) bar. Design, testing and applications. Springer, New York, pp 217–219. doi:[10.1007/978-1-4419-7982-7_6](https://doi.org/10.1007/978-1-4419-7982-7_6)
11. Nie X, Song B, Loeffler CM (2015) A novel splitting-beam laser extensometer technique for Kolsky tension bar experiment. *J Dyn Behav Mater* 1:70–74. doi:[10.1007/s40870-015-0005-7](https://doi.org/10.1007/s40870-015-0005-7)
12. Li XB, Lok TS, Zhao J, Zhao PJ (2000) Oscillation elimination in the Hopkinson bar apparatus and resultant complete dynamic stress-strain curves for rocks. *Int J Rock Mech Min Sci* 37:1055–1060. doi:[10.1016/s1365-1609\(00\)00037-x](https://doi.org/10.1016/s1365-1609(00)00037-x)
13. Zhou YX, Xia K, Li XB, Li HB, Ma GW, Zhao J, Zhou ZL, Dai F (2012) Suggested methods for determining the dynamic strength parameters and mode-I fracture toughness of rock materials. *Int J Rock Mech Min Sci* 49:105–112. doi:[10.1007/978-3-319-07713-0_3](https://doi.org/10.1007/978-3-319-07713-0_3)
14. Song B, Connelly K, Korellis J, Lu WY, Antoun BR (2009) Improved Kolsky-bar design for mechanical characterization of materials at high strain rates. *Meas Sci Tech* 20:1–8. doi:[10.1088/0957-0233/20/11/115701](https://doi.org/10.1088/0957-0233/20/11/115701)
15. Follansbee PS, Frantz C (1983) Wave propagation in the split Hopkinson pressure bar. *J Eng Mater T ASME* 105:61–66. doi:[10.1115/1.3225620](https://doi.org/10.1115/1.3225620)